Comparison of Optimal Power Flow Formulations in Active Distribution Grids

Costas Mylonas, Stavros Karagiannopoulos, *Member, IEEE,* Petros Aristidou, *Senior Member, IEEE,* Dmitry Shchetinin, *Member, IEEE,* and Gabriela Hug, *Senior Member, IEEE*

***Abstract*—Active Distribution Networks (DNs) are expected to host an increasing number of Distributed Generators (DGs) and other Distributed Energy Resources (DERs), offering new flexible sources and enabling the provision of ancillary services to system operators. Centralized DER controls that use Optimal Power Flow (OPF) methods necessitate tractable and scalable computational tools that can handle large DNs with satisfactory performance. In this paper, we compare an iterative OPF method against the standard exact AC OPF calculations in terms of the computational effort and solution quality. Furthermore, we highlight the suitability of the selected formulation to offer voltage support (VS) as an ancillary service to the transmission network. The results are demonstrated using a joint medium and low voltage grid, and show that tractable OPF formulations can unlock financial business cases for DNs that can actively participate in VS schemes.**

***Index Terms*—voltage support, centralized control, active distribution networks, OPF, backward forward sweep power flow, ancillary services, TSO, DSO**

I. Introduction

Over the last decades, modern power systems have seen a fundamental structural change through an increasing number of Distributed Energy Resources (DERs) in Medium Voltage (MV) and Low Voltage (LV) levels. In the future, the role of DNs is expected to rise, by allowing Distributed Generators (DGs) and other DERs, such as electric vehicles, Battery Energy Storage Systems (BESSs) and Controllable Loads (CLs), to provide ancillary services and support the transmission voltage levels [1].

There are various architectures to control DERs in real-time according to the available monitoring and communication infrastructure, as well as controlling capabilities. Thus, the operational schemes of active DNs can be broadly classified as *centralized* where two-way communication infrastructure is available, *distributed* where limited communication is needed so that the DERs can exchange some information, and *local* schemes where the DERs respond to local measurements without the need for communication.

Due to advances in computational power, communication capabilities and new theoretical developments in approximations of the nonlinear AC power flow equations, e.g. [2]–[4], the centralized control has lately attracted significant attention. In these schemes, a central entity uses the communication infrastructure to collect information from local DERs and calculates system-wide optimal setpoints for the controlled DERs by using optimization considering the whole network [5].

The nonlinear nature of the AC power flows calls upon Non Linear Programming (NLP) solvers to tackle the exact Optimal Power Flow (OPF) problem. All modern solvers rely on iterative schemes starting from a feasible initial operating point and stopping when no improvement is seen between successive iterations of the algorithm. The difference among them are related to the way they determine the next candidate optimal point, how they handle inequality constraints and whether they use first, or second order derivatives of the objectives and constraints [6], [7]. Apart from these algorithmic differences, the accuracy and the computational performance depend also on several other parameters such as the selection of the initial point [8], as well as the tuning parameters of the solvers.

Among the available NLP alternatives, the IPOPT method stands out as the open source state-of-the-art solver, which employs an interior-point solver using filter line search that can benefit from second-order derivative information if available [9]–[11].

Approximation methods on the contrary, rely either on linearization approaches, or convex relaxations. The accuracy of such linearization-based methods, e.g. using linear approximations around some operating point [12] or based on the Backward/Forward Sweep (BFS) power flow [13], depends heavily on the selection of the initial operating point around which we linearize, the algorithm for selecting the search space, and the convergence criteria used. The former approach, e.g. using linear approximations around some operating point [12] or based on the Backward/Forward Sweep (BFS) power flow [13], shows questionable accuracy with the quality of the result depending on the selection of the operation point around which we linearize. The latter approach, e.g. using semi-definite relaxations [3], or second-order cone programming [14], does not always find optimal or even physically meaningful solutions. In [10], several modern NLP solvers are compared in terms of computational effort and solution quality against tractable approximations. In this work, we will focus on the exact AC OPF formulation and on an iterative BFS-OPF method.

The scope of this paper is to investigate centralized optimization-based schemes for operating a DN with large shares of DERs. Considering the DSO's perspective, we assume knowledge of the branch parameters, grid topology, and

C. Mylonas, S. Karagiannopoulos and G. Hug are with the Power Systems Laboratory, ETH Zurich, 8092 Zurich, Switzerland. Email: comylona@student.ethz.ch, {karagiannopoulos | hug}@eeh.ee.ethz.ch.

P. Aristidou is with the Dept. of Electrical Engineering, Computer Engineering & Informatics, Cyprus University of Technology, 3036 Limassol, Cyprus. Email: petros.aristidou@cut.ac.cy

The authors wish to thank Dr. D. Shchetinin for sharing code regarding the AC OPF and for his valuable comments regarding optimization methods.

DER capacities. This assumption is realistic in active DNs with satisfactory data regarding their grid and advanced monitoring capabilities, e.g. via smart metering infrastructure. First, we compare different OPF formulations in terms of computational effort and quality of solution. The standard version of the AC OPF is compared against the recently proposed BFS-OPF formulation [13] in terms of objective function value and computational speed.

Then, we focus on Voltage Support (VS) as an ancillary service that can unlock new business cases to active DSOs following our previous work [15].

We will consider the VS ancillary service as described by the Swiss TSO within the BFS-OPF formulation. The DERs are given incentives to operate in such a way that they minimize the operational cost of the DSO, while keeping the voltages and the currents of the system within acceptable limits. Furthermore, the optimization considers the VS scheme, by tracking a specific voltage profile at the point of common coupling (PCC) between the TSO and DSO. Therefore, the optimal dispatch of the DERs is examined, highlighting the potential for active DNs provide services to higher voltage levels, and exploit the flexibility of inverter-based DERs.

More specifically, the contributions of this paper are twofold:

- We present various OPF formulations for active DN with multiple DERs and compare them based on optimality and computational burden. We consider different combinations of active DN measures, such as active power curtailment (APC), reactive power control (RPC), BESS and CLs.
- We select the efficient BFS OPF formulation and implement the VS framework for the case of the Swiss TSO. The economic benefits of participating in a VS scheme are demonstrated via a case study.

The remainder of the paper is organized as follows: In Section II, we present the mathematical formulations of the the standard AC OPF and the BFS OPF. Then, in Section III, we describe the active and the passive scheme of the VS established by the Swiss TSO Swissgrid and how we incorporated it into the existing BFS OPF framework. In Section IV, we introduce the case studies and the results regarding both the OPF comparison and the implementation of the VS scheme. Finally, we draw conclusions in Section V.

II. Centralized OPF Formulations

In this section, two centralized OPF schemes used to compute the optimal DER setpoints for different operating conditions are presented. Initially, we detail the modeling of the standard AC multi-period OPF problem formulation including the exact, nonlinear AC power flow equations. Then we present the BFS power flow technique and its incorporation into the OPF framework.

A. Standard AC OPF

1) Objective: The objective function minimizes the cost of DERS control and the network losses, over all of the network nodes (N_b) and branches (N_{br}) for the entire time horizon (N_{hor}). This is described by

$$\min_{\boldsymbol{u}} \sum_{t=1}^{N_{\text{hor}}} \Bigg\{ \sum_{j=1}^{N_{\text{b}}} \Big(C_{\text{P}} \cdot P_{\text{curt,j,t}} + C_{\text{Q}} \cdot Q_{\text{ctrl,j,t}} \Big) + \sum_{i=1}^{N_{\text{br}}} C_{\text{L}} \cdot P_{\text{loss,i,t}} \Bigg\} \cdot \Delta t, \tag{1}$$

where $\boldsymbol{u}$ is the vector of control variables and Δt is the length of each time period. The curtailed power of the DGs connected at node j and time t is given by $P_{\text{curt,j,t}} = P^{\text{max}}_{\text{g,j,t}} - P_{\text{g,j,t}}$, where $P^{\text{max}}_{\text{g,j,t}}$ is the maximum available active power and $P_{\text{g,j,t}}$ the active power injection of the DGs. The use of reactive power support $Q_{\text{ctrl,j,t}} = |Q_{\text{g,j,t}}|$ for each DG connected to node j and time t is also minimized; $Q_{\text{g,j,t}}$ represents the DG reactive power injection or absorption. The coefficients C_{P}, C_{Q} and C_{L} represent, respectively, the DG cost of curtailing active power, providing reactive power support and the cost of losses. The assumption that $C_{\text{Q}} \ll C_{\text{P}}$ is made, which prioritizes the use of reactive power control over active power curtailment. The losses in each branch i at time t are calculated by $P_{\text{loss,i,t}} = |I_{\text{br,i,t}}|^2 \cdot R_{\text{br,i}}$, where $I_{\text{br,i,t}}$ is the magnitude of the current flow and $R_{\text{br,i}}$ its resistance.

2) Power balance constraints: The power injections at every node j and time step t are given by

$$P_{\text{inj,j,t}} = P_{\text{g,j,t}} - P_{\text{lflex,j,t}} - (P^{\text{ch}}_{\text{B,j,t}} - P^{\text{dis}}_{\text{B,j,t}}), \tag{2a}$$

$$Q_{\text{inj,j,t}} = Q_{\text{g,j,t}} - P_{\text{lflex,j,t}} \cdot \tan(\phi_{\text{load}}), \tag{2b}$$

where $P_{\text{lflex,j,t}}$ and $P_{\text{lflex,j,t}} \cdot \tan(\phi_{\text{load}})$ are the active and reactive node demands (after control) of constant power type, with $\cos(\phi_{\text{load}})$ being the power factor of the load; $P^{\text{ch}}_{\text{B,j,t}}$ and $P^{\text{dis}}_{\text{B,j,t}}$ are respectively the charging and discharging active powers of BESS. The nodal power balance equations using the full, non-linear AC power flow are given by

$$P_{\text{inj,j,t}} = |V_{\text{bus,k,t}}| \sum_{\text{m=1}}^{N_{\text{b}}} |V_{\text{bus,m,t}}| \, (G_{\text{km}} \cos\theta_{\text{km,t}} + B_{\text{km}} \sin\theta_{\text{km,t}}), \tag{3a}$$

$$Q_{\text{inj,j,t}} = |V_{\text{bus,k,t}}| \sum_{\text{m=1}}^{N_{\text{b}}} |V_{\text{bus,m,t}}| \, (G_{\text{km}} \sin\theta_{\text{km,t}} + B_{\text{km}} \cos\theta_{\text{km,t}}), \tag{3b}$$

where $Y_{\text{km}} = G_{\text{km}} + jB_{\text{km}}$ is the nodal admittance matrix, $|V_{\text{bus,k,t}}|$, $|V_{\text{bus,m,t}}|$ are the voltage magnitudes at buses k and m respectively at time t, and $\theta_{\text{km,t}} = \theta_{\text{k,t}} - \theta_{\text{m,t}}$ is the voltage angle difference between these buses at time t.

3) Thermal loading and voltage constraints: The constraint for the current magnitude for branch i at time t is given by

$$|I_{\text{br,i,t}}| \leq I_{\text{i,max}}, \tag{4}$$

where $I_{\text{br,i,t}}$ is the branch current, and $I_{\text{i,max}}$ is the maximum thermal limit.

Similarly, the voltage constraints for each bus j and for each time step t are given by

$$V_{\text{min}} \leq |V_{\text{j,t}}| \leq V_{\text{max}}, \tag{5a}$$

$$|V_{\text{slack}}| = 1, \quad \theta_{\text{slack}} = 0, \tag{5b}$$

where V_{max} and V_{min} are respectively the upper and lower acceptable voltage limits for the magnitudes of the bus voltages $|V_{\text{bus,j,t}}|$, and $|V_{\text{slack}}|$, θ_{slack} are the fixed reference slack bus voltage magnitude and angle respectively.

4) DER constraints:

a) DG limits: In this work, without loss of generality, we only consider inverter-based DGs such as PVs. Their limits are thus given by

$$P^{\min}_{\mathrm{g,j,t}} \leq P_{\mathrm{g,j,t}} \leq P^{\max}_{\mathrm{g,j,t}}, \quad Q^{\min}_{\mathrm{g,j,t}} \leq Q_{\mathrm{g,j,t}} \leq Q^{\max}_{\mathrm{g,j,t}}, \tag{6}$$

where $P^{\min}_{\mathrm{g,j,t}}$, $P^{\max}_{\mathrm{g,j,t}}$, $Q^{\min}_{\mathrm{g,j,t}}$ and $Q^{\max}_{\mathrm{g,j,t}}$ are the upper and lower limits for active and reactive DG power at each node j and time t. These limits vary depending on the type of the DG and the control schemes implemented.

b) Controllable loads: Moreover, we consider flexible loads which can shift a fixed amount of energy consumption in time. The behavior of the loads is given by

$$P_{\mathrm{lflex,j,t}} = P_{\mathrm{l,j,t}} + \Delta P_{\mathrm{l,j,t}}, \quad \sum_{t=1}^{N_{\mathrm{hor}}} \Delta P_{\mathrm{l,j,t}} = 0, \tag{7}$$

where $P_{\mathrm{lflex,j,t}}$ is the final controlled active demand at node j and time t, $\Delta P_{\mathrm{l,j,t}}$ is the amount of increase or decrease of the load, when shifted from the known initial demand $P_{\mathrm{l,j,t}}$. We assume that the final total daily energy demand needs to remain unchanged.

c) Battery Energy Storage Systems: Finally, the constraints related to the BESS are given as

$$SoC^{\mathrm{bat}}_{\min} \cdot E^{\mathrm{bat}}_{\mathrm{cap,j}} \leq E^{\mathrm{bat}}_{\mathrm{j,t}} \leq SoC^{\mathrm{bat}}_{\max} \cdot E^{\mathrm{bat}}_{\mathrm{cap,j}}, \tag{8a}$$

$$E^{\mathrm{bat}}_{\mathrm{j,1}} = E_{\mathrm{start}}, \tag{8b}$$

$$E^{\mathrm{bat}}_{\mathrm{j,t}} = E^{\mathrm{bat}}_{\mathrm{j,t\text{-}1}} + (\eta_{\mathrm{bat}} \cdot P^{\mathrm{ch}}_{\mathrm{B,j,t}} - \frac{P^{\mathrm{dis}}_{\mathrm{B,j,t}}}{\eta_{\mathrm{bat}}}) \cdot \Delta t, \tag{8c}$$

$$0 \leq P^{\mathrm{ch}}_{\mathrm{B,j,t}} \leq P^{\mathrm{bat}}_{\max}, \quad 0 \leq P^{\mathrm{dis}}_{\mathrm{B,j,t}} \leq P^{\mathrm{bat}}_{\max}, \tag{8d}$$

$$P^{\mathrm{ch}}_{\mathrm{B,j,t}} \cdot \left(P_{\mathrm{l,j,t}} - P^{\max}_{\mathrm{g,j,t}}\right) \leq \hat{\eta}, \tag{8e}$$

$$P^{\mathrm{dis}}_{\mathrm{B,j,t}} \cdot \left(P_{\mathrm{l,j,t}} - P^{\max}_{\mathrm{g,j,t}}\right) \leq \hat{\eta}, \tag{8f}$$

where $SoC^{\mathrm{bat}}_{\min}$ and $SoC^{\mathrm{bat}}_{\max}$ are the fixed minimum and maximum per unit limits for the battery state of charge; $E^{\mathrm{bat}}_{\mathrm{cap,j}}$ is the capacity of the installed BESS at node j; and, $E^{\mathrm{bat}}_{\mathrm{j,t}}$ is the available energy at node j and at time t. The initial energy content of the BESS in the first time period is given by E_{start}, and (8c) is the model of the BESS, which updates the energy in the storage at each period t based on the BESS efficiency η_{bat}, time interval Δt and the charging and discharging active power of the BESS $P^{\mathrm{ch}}_{\mathrm{B,j,t}}$ and $P^{\mathrm{dis}}_{\mathrm{B,j,t}}$. The charging and discharging powers are defined as positive according to (8d), while (8e) and (8f) ensure that the BESS is not charging and discharging at the same time, using the small value of $\hat{\eta} = 10^{-5}$.

B. Interior Point Algorithm

For the exact AC OPF formulation we will use the interior point algorithm based on the barrier method through the IPOPT solver. Thus, we reformulate the optimization problem by modifying the objective function and the inequality constraints. More specifically, the barrier term $\zeta_k \cdot B(\boldsymbol{u})$ is added to the objective function (1), where ζ_k is a positive parameter that varies over the iterations of the algorithm and $B(\boldsymbol{u}) = -\sum_{ind}^{m} ln(-g_{ind}(\boldsymbol{u}))$ is the barrier term because it creates a barrier for the inequality constraint to become positive. The m inequality constraints, i.e. (4), (5a), (6), (8a), (8e) and (8f), are of the form $g(\boldsymbol{u}) \leq 0$. As ζ_k decreases, the solution approaches the minimum of the original problem (1).

Instead of transferring the inequality constraints to the objective function, most commonly a vector of slack variables $\boldsymbol{s} > 0$ is used to convert the inequality constraints into equality constraints, i.e. $g(\boldsymbol{u}) + \boldsymbol{s} = 0$. In this case, the barrier term becomes $B(\boldsymbol{u}) = -\sum_{ind}^{m} ln(s_{ind})$.

Thus, the final optimization problem that is solved iteratively is given by

$$\min_{\boldsymbol{u}} \sum_{t=1}^{N_{\mathrm{hor}}} \Bigg\{ \sum_{j=1}^{N_{\mathrm{b}}} \left(C_{\mathrm{P}} \cdot P_{\mathrm{curt,j,t}} + C_{\mathrm{Q}} \cdot Q_{\mathrm{ctrl,j,t}} \right) \tag{9}$$

$$+ \sum_{i=1}^{N_{\mathrm{br}}} C_{\mathrm{L}} \cdot P_{\mathrm{loss,i,t}} \Bigg\} \cdot \Delta t, - \sum_{ind}^{m} ln(s_{ind}) \tag{10}$$

$$\text{subject to} \quad h(\boldsymbol{u}) = 0, \tag{11}$$

$$g(\boldsymbol{u}) + \boldsymbol{s} = 0, \tag{12}$$

$$\boldsymbol{s} > 0, \tag{13}$$

where $h(\boldsymbol{u}) = 0$ represents the equality constraints, i.e. (2), (3), (5b), (7), (8b) and (8c).

C. BFS OPF

1) Power flow constraints: By considering the non-linear AC power balance equations (3) in the OPF problem and the inter-temporal constraints of many active measures, such as BESSs and CLs, the problem can easily become computationally complex. For this reason, the iterative BFS power flow [16] method is used in this work.

Following our previous work [13], a single iteration of the BFS power-flow method is used to replace the AC power-flow constraints in the OPF formulation. This is written as ($j = 1, \ldots N_b$):

$$I_{\mathrm{inj,j,t}} = \left(\frac{(P_{\mathrm{inj,j,t}} + jQ_{\mathrm{inj,j,t}})^*}{\bar{V}^*_{\mathrm{j,t}}} \right), \tag{14a}$$

$$\boldsymbol{I}_{\mathrm{br,t}} = \boldsymbol{BIBC} \cdot \boldsymbol{I}_{\mathrm{inj,t}}, \quad \Delta \boldsymbol{V}_{\mathrm{t}} = \boldsymbol{BCBV} \cdot \boldsymbol{I}_{\mathrm{br,t}}, \tag{14b}$$

$$\boldsymbol{V}_{\mathrm{t}} = \boldsymbol{V}_{\mathrm{slack}} + \Delta \boldsymbol{V}_{\mathrm{t}}, \tag{14c}$$

where $\bar{V}^*_{\mathrm{j,t}}$ is the voltage at node j at time t, * indicates the complex conjugate and the bar indicates that the value from the previous iteration is used; $\boldsymbol{I}_{\mathrm{inj,t}}$ and $\boldsymbol{I}_{\mathrm{br,t}}$ are respectively the vectors of injection and branch flow currents; and, $\boldsymbol{BIBC}$ (Bus Injection to Branch Current) is a matrix with ones and zeros, capturing the topology of the DN; $\Delta \boldsymbol{V}_{\mathrm{t}}$ is the vector of voltage drops over all branches; $\boldsymbol{BCBV}$ (Branch Current to Bus Voltage) is a matrix with the complex impedance of the lines as elements (including mutual coupling); and $\boldsymbol{V}_{\mathrm{slack}}$ is the voltage in per unit at the slack bus (here assumed to be $1{<}0^{\circ}$);

2) Iterative Solution Algorithm: After the optimal setpoints of the OPF problem are obtained, the exact BFS power flow is performed to update the operating point and project it into the feasible domain of the exact power flow equations. This new

operating point will be used as input to the subsequent iteration of the BFS-OPF problem, and this loop will be repeated until convergence in terms of voltage magnitude mismatch. The iterative algorithm is explained in detail in [13].

III. Voltage Support Scheme in Switzerland

In this section, we describe the active and passive models introduced by the Swiss TSO. According to this scheme a DSO whose network is directly connected to the TN can decide if the corresponding transformers are treated as active or passive participants. A detailed description of this ancillary service within an optimization framework is found in [15].

A. Passive Participation in VS

In the passive role, the DN is economically encouraged to limit the reactive energy exchange E_{Q}, measured every 15 minutes ($0.25h$), to the symmetrical cost-free region shown in the left part of Fig. 1.

The tolerance threshold $E_{\mathrm{Q}}^{\mathrm{lim}}$ in MVAr refers to the amount of reactive energy exchanged, and operates as a threshold for the cost-free region. The reactive energy exchanged beyond this tolerance threshold is given by

$$E_{\mathrm{Q,billed}} = \begin{cases} |E_{\mathrm{Q}}| - E_{\mathrm{Q}}^{\mathrm{lim}}, & \text{if } |E_{\mathrm{Q}}| > E_{\mathrm{Q}}^{\mathrm{lim}} \\ 0, & \text{otherwise} \end{cases}, \tag{15}$$

where E_{Q} is the net reactive energy exchanged with the TN in MVAr (15-minute meter value), $E_{\mathrm{Q}}^{\mathrm{lim}}$ is the reactive energy limit in MVAr (for both inductive and capacitive ranges); and $E_{\mathrm{Q,billed}}$ is the additional reactive energy to be billed in MVAr. The cost for the additional reactive energy is calculated by multiplying the 15-minute reactive energy value by the specific tariff, i.e, $cost_{\mathrm{passive}} = c_{\mathrm{passive,noncm}} \cdot E_{\mathrm{Q,billed}}$, where $c_{\mathrm{passive,noncm}}$ is the tariff in CHF/MVAr according to [17]. The final cost for this 15-minute period is given by $cost_{\mathrm{passive}}$.

The limits $E_{\mathrm{Q,lim}}^{\mathrm{pf}}$ and $E_{\mathrm{Q,lim}}^{\mathrm{tr}}$ shown in Fig. 1 depend on the predefined power factor limit pf_{lim} (e.g. Swissgrid uses $pf_{\mathrm{lim}} = 0.9$), the net active energy exchanged E_{P} in MWh (15-minute meter value) and the transformer's parameters. They are given by $\pm E_{\mathrm{Q,lim}}^{\mathrm{pf}} = tan(arccos(0.90)) \cdot |E_{\mathrm{P}}| = 0.4843 \cdot |E_{\mathrm{P}}|$, and $\pm E_{\mathrm{Q,lim}}^{\mathrm{tr}} = \frac{u_{\mathrm{sc}}}{100} \cdot S_{\mathrm{N}} \cdot 0.25h$, where u_{sc} is the transformer's short-circuit voltage in percentage, and S_{N} is the transformer's nominal apparent power in MVA. Finally, the value $E_{\mathrm{Q}}^{\mathrm{lim}}$ used in (15) can be calculated by

$$\pm E_{\mathrm{Q}}^{\mathrm{lim}} = \max\{E_{\mathrm{Q,lim}}^{\mathrm{pf}}, E_{\mathrm{Q,lim}}^{\mathrm{tr}}\}. \tag{16}$$

B. Active Participation in VS

In the active role, the DSO can utilize its available reactive energy capabilities to support the TN's voltage V_{m} when requested by the TSO. For this purpose, the TSO sends an individual reference voltage setpoint V_{set} to every active participant which is calculated off-line, based on the Day-Ahead Reactive Planning (DARP) problem, i.e. an OPF problem in the TN using forecasted data.

Depending on the actual voltage V_{m}, the participant has to inject or consume reactive energy. The reactive energy exchange is considered to be compliant if it contributes to reach the setpoint voltage V_{set}. In the right part of Fig. 1, it can be noticed that if V_{m} is smaller than V_{set} and the participant injects reactive energy into the TN, its behavior is compliant and the participant is getting paid for the delivered reactive energy. In contrast, the participant is penalized for the amount of the injected reactive energy if V_{m} is higher than V_{set}, because the additional reactive energy destabilizes the system. A margin ϵ between the setpoint and the actual voltage is allowed for settlement, in favor of the participant.

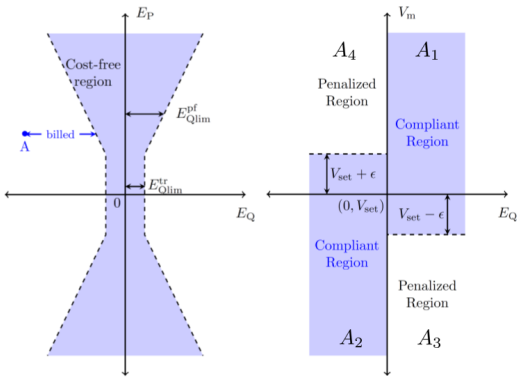

Fig. 1. Passive (left) and active (right) participation in the VS scheme of the Swiss TN.

The compliant areas shown in Fig. 1 can by calculated by $A_1 = \{E_{\mathrm{Q}} \geq 0, V_{\mathrm{m}} - V_{\mathrm{set}} \geq -\epsilon\}$ $A_2 = \{E_{\mathrm{Q}} \leq 0, V_{\mathrm{m}} - V_{\mathrm{set}} \leq \epsilon\}$ and the non-compliant by $A_3 = \{E_{\mathrm{Q}} \geq 0, V_{\mathrm{m}} - V_{\mathrm{set}} \leq -\epsilon\}$ and $A_4 = \{E_{\mathrm{Q}} \leq 0, V_{\mathrm{m}} - V_{\mathrm{set}} \geq \epsilon\}$.

The resulting cost or revenue depends on the absolute value of the reactive energy exchanged, multiplied by the corresponding tariffs. This is described by

$$cost_{\mathrm{active}} = \begin{cases} -c_{\mathrm{active,cm}} \cdot |E_{\mathrm{Q}}|, & \text{if } x \in A_1 \cup A_2 \\ +c_{\mathrm{active,noncm}} \cdot |E_{\mathrm{Q}}|, & \text{if } x \in A_3 \cup A_4 \end{cases}, \tag{17}$$

where $cost_{\mathrm{active}}$ is the final remunerated/billed amount in CHF for the 15-minute period, while $c_{\mathrm{active,cm}}$ and $c_{\mathrm{active,noncm}}$ are the reactive energy tariffs in CHF/MVAr according to [17] for the compliant and in the non-compliant case, respectively.

C. Overall BFS-OPF formulation

In this part, we summarize the final BFS-OPF formulation that considers combines the BFS OPF introduced in Section II and the VS scheme explained in Section III.

The overall OPF formulation, is given by

$$\min_{\boldsymbol{u}} \sum_{t=1}^{N_{\mathrm{hor}}} \Bigg\{ \sum_{j=1}^{N_{\mathrm{b}}} \Big(C_{\mathrm{P}} \cdot P_{\mathrm{curt,j,t}} + C_{\mathrm{Q}} \cdot Q_{\mathrm{ctrl,j,t}} \Big) + \sum_{i=1}^{N_{\mathrm{br}}} C_{\mathrm{P}} \cdot P_{\mathrm{loss,i,t}} + \sum_{k \in N_{\mathrm{passive}}} cost_{\mathrm{passive,t,k}} + \sum_{k \in N_{\mathrm{active}}} cost_{\mathrm{active,t,k}} \Bigg\} \cdot \Delta t,$$
$$\text{subject to } (2), (4), (5), (6), (7), (8), (14), \tag{18}$$

where N_{passive} is the set of all passive participants in the grid,and N_{active} the set of all active participants.

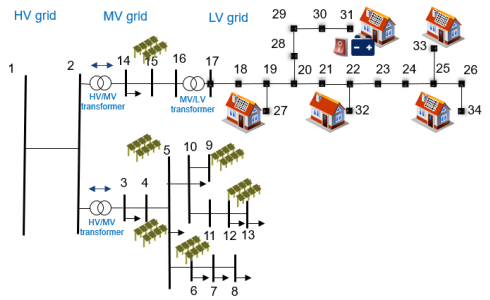

Fig. 2. Joint MV and LV European grids [18] connected to the transmission voltage level through a Thévenin equivalent.

IV. Case Studies - Results

To analyze the performance of the proposed centralized scheme, we merged the typical European MV and LV grids [18], as sketched in Fig. 2. We consider two feeders connecting to the HV network. In the upper one, we model in detail the LV grid with the operational flexibility of each rooftop PV unit, while the second aggregates the LV grid similar to most studies. The TN is modeled by a Thévenin equivalent at Node 1 in order to investigate the influence of the DN to the VS scheme. Its impedance is selected relatively high and represents a weak 220 kV grid. The installed PV capacities in the MV and LV grids are summarized as follows: PV nodes = [4, 5, 6, 9, 13, 15, 27, 31, 33, 34] and PV installed capacity (MVA) = [1, 1, 1, 1, 0.1, 0.15, 0.1, 0.12]. Furthermore, we consider at node 31 a BESS of 26 kWh and a CL of 10 kW. In this work, we only consider balanced, single-phase system operation. The normalized PV injection profiles are taken from PV stations at the area of Switzerland, following [19] and the load data are taken by [18].

The operational costs are assumed to be $c_{\mathrm{P}} = 3\frac{CHF}{kWh}$, $c_{\mathrm{Q}} = 0.003\frac{CHF}{kVarh}$ and $c_{\mathrm{L}} = 0.3\frac{CHF}{kWh}$. The tariffs for the active and passive participation in VS for 2018 published by Swissgrid [17] are: $c_{\text{passive,noncm}} = c_{\text{active,noncm}} = 0.0151\frac{CHF}{kVarh}$ and $c_{\text{active,cm}} = 0.003\frac{CHF}{kVarh}$.

A. Comparison of OPF Formulations

In the first part of the results, we compare the solution quality and computational effort of the BFS-OPF formulation against the standard AC OPF problem, i.e. using the exact power flow equations (3a), (3b). The comparison is performed in terms of the objective function value and the required solving time. Please note that for the BFS-OPF case, this refers to the sum of time needed for all iterations until convergence. Furthermore, we consider another AC OPF case, where additional information is provided to the solver in order to speed up the calculations. More specifically, the results of the following setups are considered:

- Method 1: BFS-OPF using YALMIP [20] and Gurobi [21] as the interface platform and solver, respectively.
- Method 2: Standard AC OPF using the nonlinear and non-convex power flow equations, and IPOPT [9] as the solver of the non-convex problem.

TABLE I
Objective function value for the MV-LV grid.

Objective Function Value (kCHF)	APC	+RPC	+BESS	+CL
Method 1	2.37	2.24	2.18	2.12
Method 2	2.24	2.11	2.06	2.05
Method 3	2.24	2.11	2.06	2.05

TABLE II
Solving time for the MV-LV grid.

Solving Time (sec)	APC	+RPC	+BESS	+CL
Method 1	2.59	2.66	2.67	2.79
Method 2	21.41	41.63	46.35	48.68
Method 3	1.92	2.15	2.72	2.75

- Method 3: Standard AC OPF similar to the previous case, but also providing the gradient and Hessian of the objective function and the Jacobian of the nonlinear constraints, as well as the Hessian of the Lagrangian. The functions to compute these functions are taken from [22].

We simulate 24-hour problems, using the joint Cigré MV-LV grid comprising 33 nodes.

Tables I and II show the objective function value and solution solving time (solver's time), respectively, for the OPF calculations. We present results adding one active control measure at a time, i.e. the last column includes APC, RPC, BESS and CL. First, we observe that both AC OPF formulations result in the same solutions for all cases. Their difference relate to the needed computational time, since Method 3 runs significantly faster due to the increased information provided, as seen in Table II. Supplying the exact second derivatives of both the objective and all constraints saves gradient based solvers such as IPOPT from using quasi-newton numerical approximations of the second derivatives which requires computational effort.

The BFS-OPF (Method 1) results in approximately 5% higher objective function values. However, the needed solving time is decreased up to 40 times compared to the AC OPF formulation of Method 2.

Overall, we observe that the BFS-OPF results are close to the AC OPF. The efficiency of the BFS algorithm is shown in the reduction of the needed solving time, justifying the use of the BFS-OPF in cases where tractability is of crucial importance.

B. Passive Participation

In this part of the results we examine the case, where the DN follows a passive participation in the VS scheme. We compare the results from a) running an OPF-based scheme as described in Section II without providing VS to the TN, and b) running the same OPF-based scheme, following in addition the passive VS participation, as explained in Section III-A.

The VS scheme incurs costs when the reactive power exchange exceeds the varying limit that is calculated by (16). During noon hours the OPF that considers the VS scheme manages to reach the cost-free region, by requiring less reactive power from the TN. The change of the operating points for the hour 13:00 is shown in Fig. 3. The DN is able

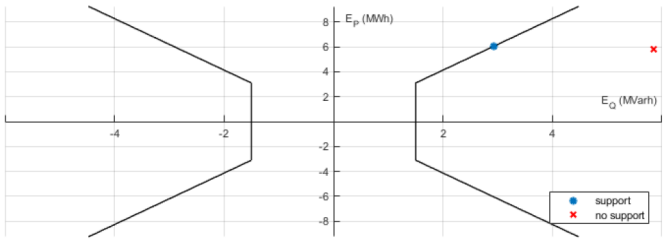

Fig. 3. Cost-free and penalization regions for the passive VS participation.

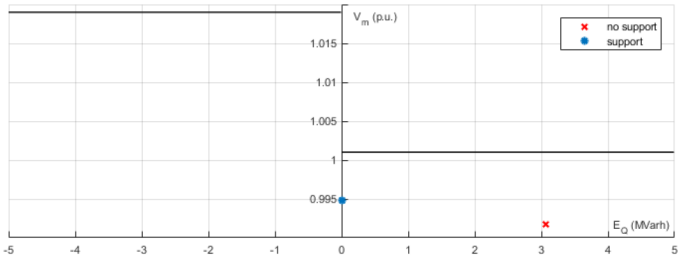

Fig. 4. Compliant and penalization regions for the active VS participation.

is reduce only the reactive energy exchange, in order to avoid the cost penalization without interfering with the active energy exchange.

C. Active Participation

In this part, the DN selects the active participation to the VS. The focus here is to use the operational flexibility of the DERs located in both MV and LV in order to track a voltage magnitude profile provided by the TSO. This voltage reference profile which is derived by the TSO Day-ahead Reactive Planning (DARP) procedure, is assumed flat at 1.01 p.u. with a 9% tolerance, i.e. $\epsilon = 0.009$ p.u. We compare the results from a) running an OPF-based scheme as described in Section II without providing VS to the TN, and b) running the same OPF-based scheme, following in addition the passive VS participation, as explained in Section III-B.

Fig. 4 shows the pair of the measured voltage and the daily reactive energy exchange for the hour 13:00. We observe that the OPF case that does not consider the active VS scheme results in a voltage increase, indicating that less reactive power is required by the TN, i.e. more reactive power is produced locally within the DN. However, the voltage needs to be further increased in order to reach the compliant area and this is indicated by the change of the operating points.

V. Conclusion

The increasing controllability and observability in MV and LV grids lay the ground for a more efficient TSO-DSO coordination. In this paper, we first compare the BFS-OPF against the standard AC OPF with respect to the accuracy and the solution time. We quantified the missmatches between the BFS-OPF and interior-point solvers and highlighted the benefit of supplying the solver with exact second derivative information. Then, we incorporate the Swiss VS scheme into the BFS OPF formulation to investigate the provision of this ancillary service to the TN. We have demonstrated through the case studies used that the BFS-OPF provides a tractable tool for centralized control approaches, and that a DSO can optimize its grid operation safely, while at the same time it can assist the TN in terms of tracking a derived voltage profile.

References

[1] N. Hatziargyriou, O. Vlachokyriakou, T. Van Cutsem, J. Milanović, P. Pourbeik, C. Vournas, M. Hong, R. Ramos, J. Boemer, P. Aristidou, V. Singhvi, J. dos Santos, and L. Colombari, "Task Force on Contribution to Bulk System Control and Stability by Distributed Energy Resources connected at Distribution Network," IEEE PES, Tech. Rep., 2017.

[2] F. Capitanescu, "Critical review of recent advances and further developments needed in ac optimal power flow," *Electric Power Systems Research*, vol. 136, pp. 57–68, 2016.

[3] J. Lavaei and S. H. Low, "Zero duality gap in optimal power flow problem," *IEEE Transactions on Power Systems*, vol. 27, no. 1, pp. 92–107, 2012.

[4] D. K. Molzahn and I. A. Hiskens, "Sparsity-Exploiting Moment-Based Relaxations of the Optimal Power Flow Problem," *IEEE Transactions on Power Systems*, vol. 30, no. 6, pp. 3168–3180, Nov 2015.

[5] P. Fortenbacher, M. Zellner, and G. Andersson, "Optimal sizing and placement of distributed storage in low voltage networks," in *Proceedings of the 19th Power Systems Computation Conference (PSCC), Genova*, Jun 2016.

[6] A. Castillo and R. P. O'Neill, "Survey of approaches to solving the acopf," *Federal Energy Regulatory Commission, Tech. Rep*, 2013.

[7] ——, "Computational performance of solution techniques applied to the acopf," *Federal Energy Regulatory Commission, Optimal Power Flow Paper*, vol. 5, 2013.

[8] M. Gertz, J. Nocedal, and A. Sartenar, "A starting point strategy for nonlinear interior methods," *Applied mathematics letters*, vol. 17, no. 8, pp. 945–952, 2004.

[9] COIN-OR, "Introduction to ipopt: A tutorial for downloading, installing, and using ipopt," 2015, https://projects.coin-or.org/Ipopt/browser/stable/3.11/Ipopt/doc/documentation.pdf?format=raw.

[10] D. Shchetinin, T. T. De Rubira, and G. Hug, "On the construction of linear approximations of line flow constraints for ac optimal power flow," *IEEE Transactions on Power Systems*, vol. 34, no. 2, pp. 1182–1192, March 2019.

[11] A. Wächter and L. T. Biegler, "On the implementation of an interior-point filter line-search algorithm for large-scale nonlinear programming," *Mathematical programming*, vol. 106, no. 1, pp. 25–57, 2006.

[12] S. Bolognani and F. Dörfler, "Fast Power System Analysis via Implicit Linearization of the Power Flow Manifold," pp. 402–409, 2015.

[13] S. Karagiannopoulos, P. Aristidou, and G. Hug, "Data-driven local control design for active distribution grids using off-line optimal power flow and machine learning techniques," *IEEE Transactions on Smart Grid*, vol. 10, no. 6, pp. 6461–6471, Nov 2019.

[14] R. A. Jabr, "Radial distribution load flow using conic programming," *IEEE Transactions on Power Systems*, vol. 21, no. 3, pp. 1458–1459, Aug 2006.

[15] S. Karagiannopoulos, C. Mylonas, P. Aristidou, and G. Hug, "Active Distribution Grids Providing Voltage Support: The Swiss Case," *IEEE Transactions on Smart Grid (submitted)*, 2019.

[16] J. H. Teng, "A direct approach for distribution system load flow solutions," *IEEE Transactions on Power Delivery*, vol. 18, no. 3, pp. 882–887, 2003.

[17] Swissgrid, "Tariffs," 2019, https://www.swissgrid.ch/dam/swissgrid/customers/topics/tariffs/Tabelle-Tarife-en.pdf.

[18] K. Strunz, E. Abbasi, C. Abbey, C. Andrieu, F. Gao, T. Gaunt, A. Gole, N. Hatziargyriou, and R. Iravani, *Benchmark Systems for Network Integration of Renewable and Distributed Energy Resources*. CIGRE, Task Force C6.04, 2014.

[19] S. Karagiannopoulos, P. Aristidou, L. Roald, and G. Hug, "Operational Planning of Active Distribution Grids under Uncertainty," in *IREP 2017, X Bulk Power Systems Dynamics and Control Symposium*, Aug 2017.

[20] J. Löfberg, "Yalmip : A toolbox for modeling and optimization in matlab," in *In Proceedings of the CACSD Conference*, Taiwan, 2004.

[21] I. Gurobi Optimization, "Gurobi optimizer reference manual," 2016. [Online]. Available: http://www.gurobi.com

[22] C. E. M.-S. R. D. Zimmerman and R. J. Thomas, "MATPOWER: Steady-State Operations, Planning and Analysis Tools for Power Systems Research and Education," *Power Systems, IEEE Transactions*, vol. 26, pp. 12–19, 2011.